Journal of Power Sources 196 (2011) 2621–2626

Contents lists available at ScienceDirect

Journal of Power Sources

journal homepage: www.elsevier.com/locate/jpowsour

Pt nanoparticles supported on WO_3/C hybrid materials and their electrocatalytic activity for methanol electro-oxidation

Zhiming Cui, Ligang Feng, Changpeng Liu, Wei Xing*

State Key Laboratory of Electro-analytical Chemistry, Changchun Institute of Applied Chemistry, Jilin Province Key Laboratory of Low Carbon Chemical Power, Graduate School of the Chinese Academy of Sciences, 5625 Renmin Street, Changchun, Jilin 130022, P.R. China

ARTICLE INFO

Article history:
Received 24 August 2010
Accepted 31 August 2010
Available online 8 September 2010

Keywords:
Direct methanol fuel cell
Methanol electro-oxidation
Phosphotungstic acid
Tungsten trioxide

ABSTRACT

A simple and novel method for the preparation of WO_3/C is presented. This method includes the adsorption and decomposition of phosphotungstic acid (PWA) on carbon. For the purpose of comparison, WO_3/C is also prepared by a conventional method using sodium tungstate as the precursor. These two WO_3/C species are denoted as WO_3/C-1 and WO_3/C-2, respectively. It is shown from transmission electron microscopy (TEM) that the WO_3 particles in WO_3/C-1 present a more even distribution and smaller particle size than those in WO_3/C-2. Pt particles dispersed on WO_3/C-1 display the characteristic diffraction peaks of Pt in the face-centered cubic phase. Cyclic voltammetry and chronoamperometry show that the Pt–WO_3/C-1 catalyst exhibits much better methanol oxidation activity than the Pt–WO_3/C-2 and Pt/C catalysts. This significant improvement in catalytic performance may be attributed to the hydrogen spillover effect and the uniform distribution of Pt and WO_3 particles.

1. Introduction

The direct methanol fuel cell (DMFC) is generally considered to be a good candidate for future energy-generating devices, particularly for portable electronics and vehicular applications, due to its high specific energy at low operating temperatures and its ease of handling as a clean liquid fuel [1–3]. However, there are still several issues that must be overcome before its commercialization. Among them, the most critical is the poor kinetics of the methanol oxidation reaction on conventional anode catalyst materials. Therefore, intensive research has been carried out in the past decade on Pt-based multicomponent catalysts to improve the poison tolerance of anode catalysts with the ultimate goal of creating cost-effective catalysts for practical fuel cells. Metals including ruthenium, osmium, iridium, rhodium, tin, and others have been shown to improve the catalytic activity of Pt either by modifying the surface chemistry to produce a bifunctional material, or by modifying the electronic properties of Pt. In the bifunctional mechanism, the alloyed metal forms surface oxides at much lower potentials than Pt [4,5]. By means of the electronic mechanism (or the ligand effect), the alloyed metal modifies the electronic structure of Pt, resulting in a lower bond strength of the species adsorbed on Pt [6–9].

Tungsten trioxide (WO_3) is known to be able to form a hydrogen tungsten bronze (H_xWO_3) compound in acid solution which is both nonstoichiometric and electrically conducting. The compound can facilitate dehydrogenation during methanol oxidation and lighten the CO poisoning of Pt catalyst [10–12]. Previous studies have shown that Pt and PtRu catalysts supported on WO_3 have extremely high activity towards the electro-oxidation of CO [13], methanol [14–17], ethanol [18] and formic acid [19,20]. However, WO_3 has a low specific surface area and conductivity, which limits its application in DMFCs.

In the present work, a WO_3/C hybrid material is fabricated by the adsorption and decomposition of phosphotungstic acid (PWA) on carbon and the resulting WO_3/C material is used as a catalyst support for the purpose of producing high-activity Pt–WO_3/C catalysts.

2. Experimental

2.1. Materials

Vulcan XC-72 carbon black was purchased from the Cabot Corporation. Chloroplatinic acid hydrate, phosphotungstic acid (Keggin-type) and sodium tungstate was bought from the Aldrich Chemical Co. Deionized water (18.23 MΩ) was produced by a Milli-Q ultrapure system (Millipore Ltd., USA).

2.2. Preparation of WO_3/C and Pt–WO_3/C catalysts

Two catalyst support materials were fabricated for this study. The first one was prepared by the adsorption and decomposition of phosphotungstic acid (PWA) on carbon, denoted as WO_3/C-1. This

* Corresponding author. Tel.: +86 431 5262223; fax: +86 431 5262223.
E-mail address: xingwei@ciac.jl.cn (W. Xing).

0378-7753/$ – see front matter © 2010 Elsevier B.V. All rights reserved.
doi:10.1016/j.jpowsour.2010.08.118

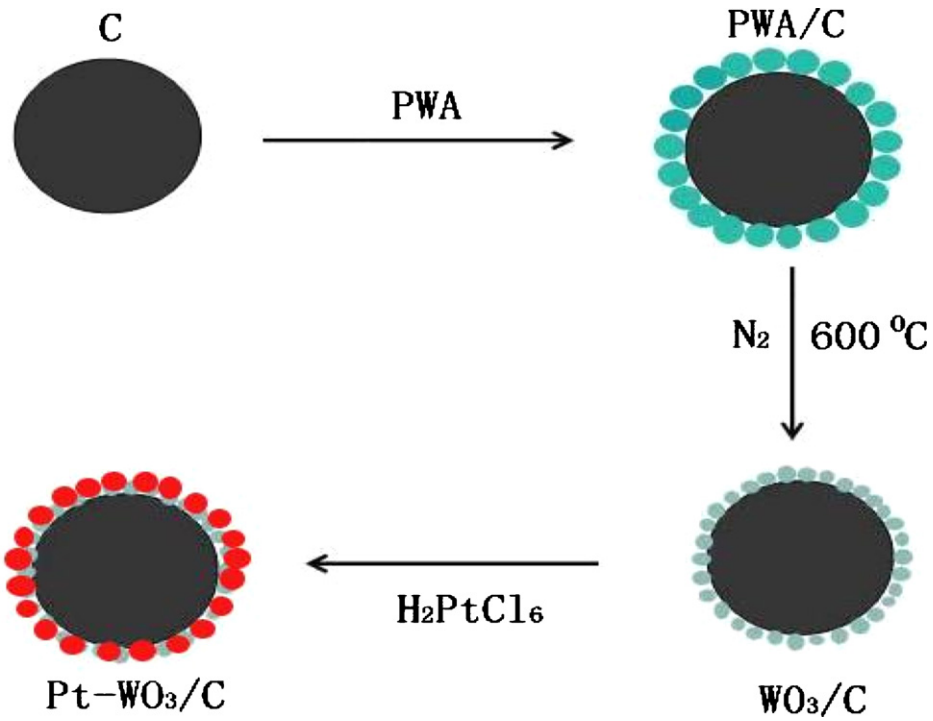

Fig. 1. Schematic diagram for the preparation of the Pt–WO_3/C-1 catalyst.

novel procedure is illustrated in Fig. 1. First, 1 g carbon powder was added to 50 ml of PWA solution (20 mg ml^{-1}) and kept at room temperature for 72 h under vigorous agitation. Then, the suspension was filtered and dried at 80 °C for 6 h to obtain PWA/C. Finally, the PWA/C was calcined at 600 °C under the nitrogen protection for 6 h to give a decomposition product of tungsten trioxide supported on carbon (WO_3/C) [21].

The second support material, denoted as WO_3/C-2, was prepared as follows. Sodium tungstate was added to a carbon suspension under vigorous agitation before the solution was heated to 80 °C. With the addition of excessive hydrochloric acid, a tungstenic acid deposit was formed. After the reaction proceeded for 6 h, the suspension was filtered, washed and dried at 80 °C in a vacuum oven. To obtain stable WO_3/C, the resultant was transferred into a tubular oven and heat-treated at 500 °C for 6 h under the protection of a nitrogen atmosphere.

Preparation of Pt–WO_3/C was done as follows. First, an appropriate amount of H_2PtCl_6 solution was thoroughly mixed with the WO_3/C support by sonication and agitation. Then the mixture was kept at 90 °C, and hydrogen was introduced for 5 h. Subsequently, the suspension was filtered and washed with deionized water, and then dried at 80 °C for 6 h to obtain the Pt–WO_3/C-1 (20 wt% Pt) and Pt–WO_3/C-2 (20 wt% Pt) catalysts. Pt/C (20 wt% Pt) was prepared in the same way.

2.3. Physicochemical characterization of catalysts

The size and morphology of the WO_3/C and Pt–WO_3/C catalysts were characterized by TEM (JEOL JEM2010). The bulk compositions of the prepared catalysts were evaluated by energy dispersive X-ray analysis with a scanning electron microscope (JEOL JAX-840). X-ray photoelectron spectroscopy (XPS) measurements were carried out by a Kratos XSAM-800 spectrometer with a Mg Kα radiator. X-ray diffraction spectra were measured by a Philips PW1700 diffractometer with a Cu Kα (λ = 1.5405 Å) radiation source operating at 40 kV and 30 mA.

2.4. Electrochemical measurements

Electrochemical measurements were carried out with an EG&G mode 273 potentiostat/galvanostat and a conventional three-electrode test cell. The catalyst ink was prepared by ultrasonically dispersing the mixture of 5 mg catalysts, 1 ml ethanol, and 50 μl 5 wt% Nafion solutions. 10 μl catalyst inks were pipetted and spread on the glassy carbon disk. Large surface area Pt foil served as counter electrode, and a silver–silver chloride electrode was used as the reference electrode. All electrolyte solutions were deaerated by high-purity nitrogen for 15 min prior to any measurement. For chronoamperometry, the electrode potential was fixed at 0.6 V (vs. Ag/AgCl). The specific surface area of Pt in the catalysts was measured electrochemically by oxidation of pre-adsorbed CO (CO_{ad}) in a 0.5 M H_2SO_4 solution at a scan rate of 20 mV s^{-1}. CO was purged into the 0.5 M H_2SO_4 solution for 30 min to allow the complete adsorption of CO onto the catalyst when the working electrode was kept at 0 mV (vs. Ag/AgCl). Excess CO in the electrolyte was then purged out with N_2 for 10 min. The amount of CO_{ad} was evaluated by integration of the CO_{ad} stripping peak, and corrected by the electric double-layer capacitance. The specific surface area of the Pt metal was estimated to be a monolayer of linearly adsorbed CO and the Coulombic charge necessary for oxidation was 420 μC cm^{-2} [22,23].

3. Results and discussion

3.1. TEM, EDX, XPS and XRD analyses

TEM images of WO_3/C-1 and WO_3/C-2 in Fig. 2 clearly show that the WO_3 particles in the WO_3/C-1 sample are much better distributed and have a smaller particle size (2–3 nm) than those in the WO_3/C-2 sample. This can be explained as follows.

The surface of carbon contains different oxygen-containing groups, which can be protonated by a strong acid, such as PWA. The adsorption of PWA on carbon materials can be ascribed to an

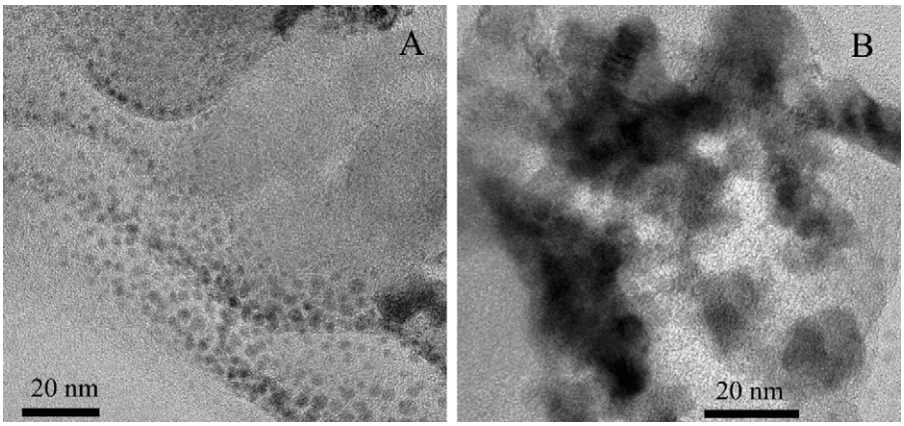

Fig. 2. TEM images of (A) WO_3/C-1 and (B) WO_3/C-2.

acid–base reaction [24].

$$MOH_2^+ + (HPA_n)^- = MOH_2^+(HPA_n)^- \quad (1)$$

PWA is uniformly dispersed onto the carbon support due to the interaction between carbon and PWA. PWA/C is calcined in N_2 to give a decomposition product of highly dispersed WO_3/C.

Fig. 3 gives the TEM images of Pt–WO_3/C-1, Pt–WO_3/C-2 and Pt/C catalysts and the corresponding histograms of the Pt particle diameters, as well. It can be seen from the TEM images that the Pt particles on the WO_3/C support are smaller and more uniformly dispersed than those on carbon support. The average sizes of the Pt particles in the Pt–WO_3/C-1, Pt–WO_3/C-2 and Pt/C catalysts are estimated from their histograms as being approximately 3.2, 3.5, and 3.9 nm, respectively, indicating that the introduction of WO_3 can inhibit the aggregation of Pt particles.

The composition of the bulk catalysts is determined through energy dispersive X-ray (EDX) analysis. The weight content of Pt in the Pt–WO_3/C-1 catalysts is 20.6% and the Pt/W atomic ratio is estimated to be 1.67; while the weight content of Pt in Pt–WO_3/C-2 catalysts is 21.2% and the Pt/W atomic ratio is estimated to be 1.71. The weight content of Pt in the Pt/C catalysts is 19.7%.

The XRD patterns for Pt–WO_3/C-1, Pt–WO_3/C-2, and Pt/C catalysts are shown in Fig. 4, from which the crystalline lattice fringes of the samples are confirmed. For Pt–WO_3/C-1 and Pt–WO_3/C-2, the diffraction peaks at 39°, 46°, 68°, and 81°, are due to the Pt (1 1 1), (2 0 0), (2 2 0), and (3 1 1) planes, respectively, and confirm that these catalysts exhibit the Pt fcc structure. The diffraction peaks at 33°, 40°, 49°, 54°, 61°, and 76° correspond to the monoclinic phases of WO_3 [26]. The peak observed at 24° is attributed to the hexagonal graphite structure (0 0 2).

Fig. 5 plots the Pt 4f and W 4f XPS results. The binding energies (BE) of all of the peaks are referenced to a C 1s value of 284.6 eV. All samples demonstrate similarly asymmetric peaks, indicating different Pt oxidation states. Compared with the peak ($4f_{7/2}$) at 71.2 for Pt/C, the peaks ($4f_{7/2}$) for Pt–WO_3/C-1 and Pt–WO_3/C-2 shift positively by 0.4 and 0.3 eV, respectively, reflecting strong interactions between Pt and WO_3. This phenomenon is a symbol of a strong "metal–support interaction" between Pt and WO_3. This interac-

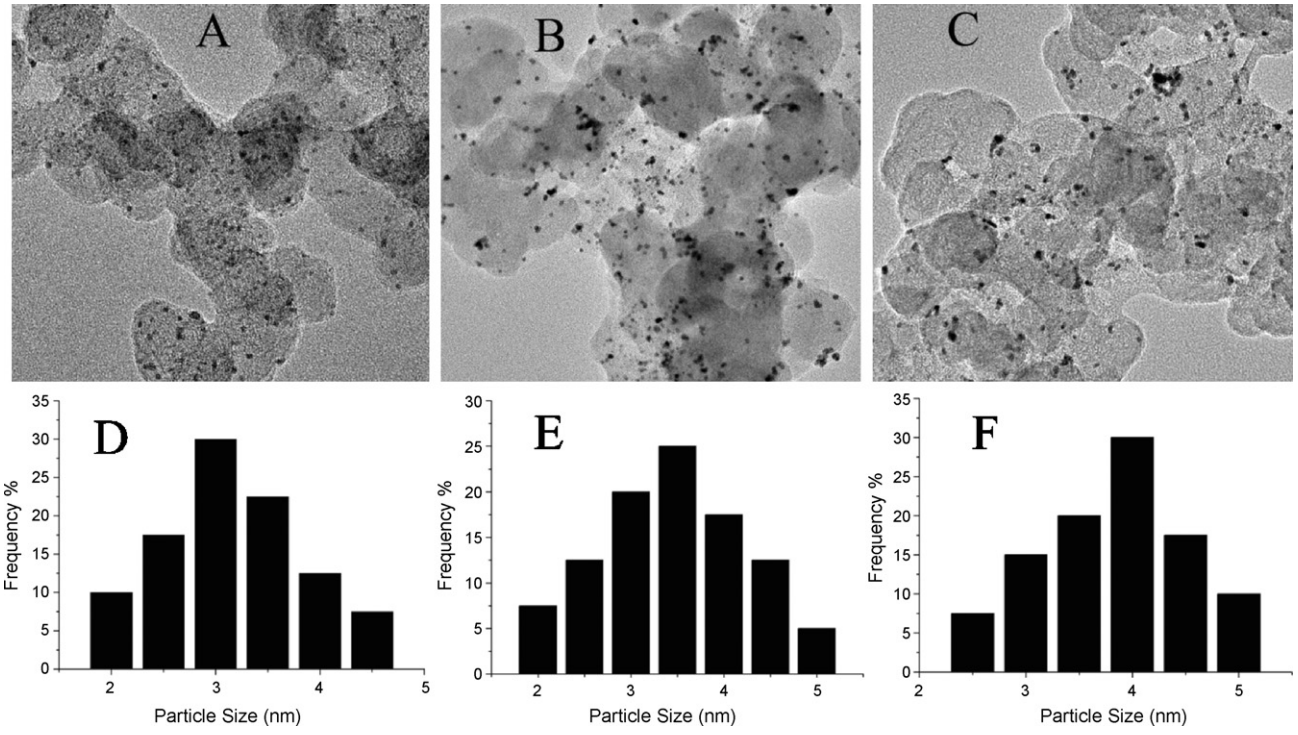

Fig. 3. TEM images of the (A) Pt–WO_3/C-1, (B) Pt–WO_3/C-2, and (C) Pt/C, and Pt particle diameters histograms of (D) Pt–WO_3/C-1, (E) Pt–WO_3/C-2, and (F) Pt/C catalysts.

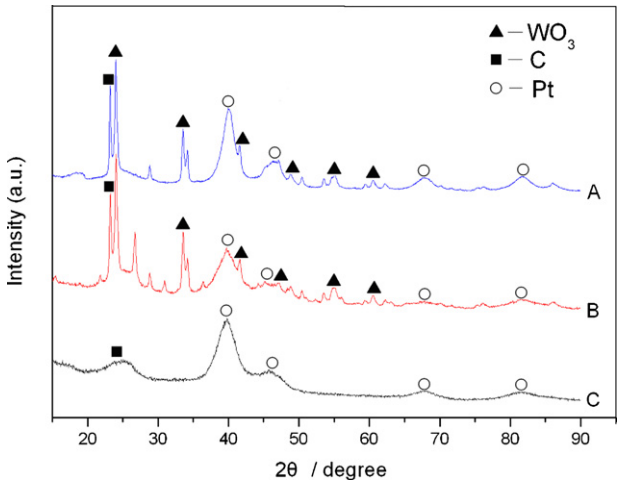

Fig. 4. XRD patterns for the (A) Pt–WO_3/C-1, (B) Pt–WO_3/C-2, and (C) Pt/C.

tion can modify the electronic and catalytic properties of metal nanoparticles and lead to the electrochemical activation of both dispersed metal and oxide. The W (4f) region of the XPS spectrum of both the Pt–WO_3/C-1 and Pt–WO_3/C-2 samples is also shown in Fig. 5. The W ($4f_{7/2}$) and W ($4f_{5/2}$) peaks for the Pt–WO_3/C catalyst are located at 34.9 and 37.1 eV, respectively, which shows that W predominantly exists in the form of tungsten oxide [25] on the surface of the Pt–WO_3/C catalyst. There might be a small fraction of W^{5+} in both the Pt–WO_3/C-1 and Pt–WO_3/C-2 samples.

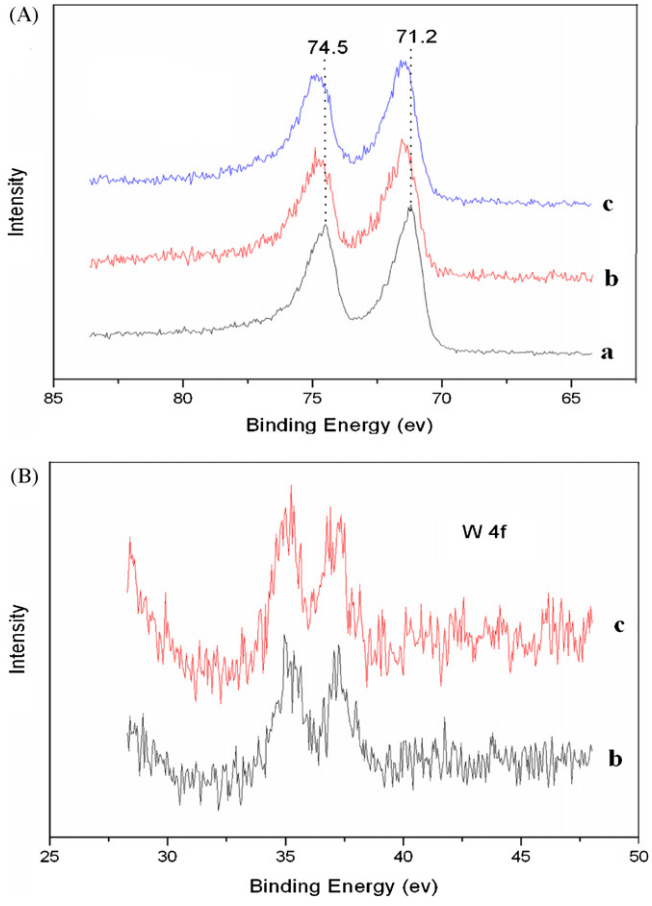

Fig. 5. Pt (4f) and W (4f) XPS spectrum of the (a) Pt/C, (b) Pt–WO_3/C-2, and (c) Pt–WO_3/C-1.

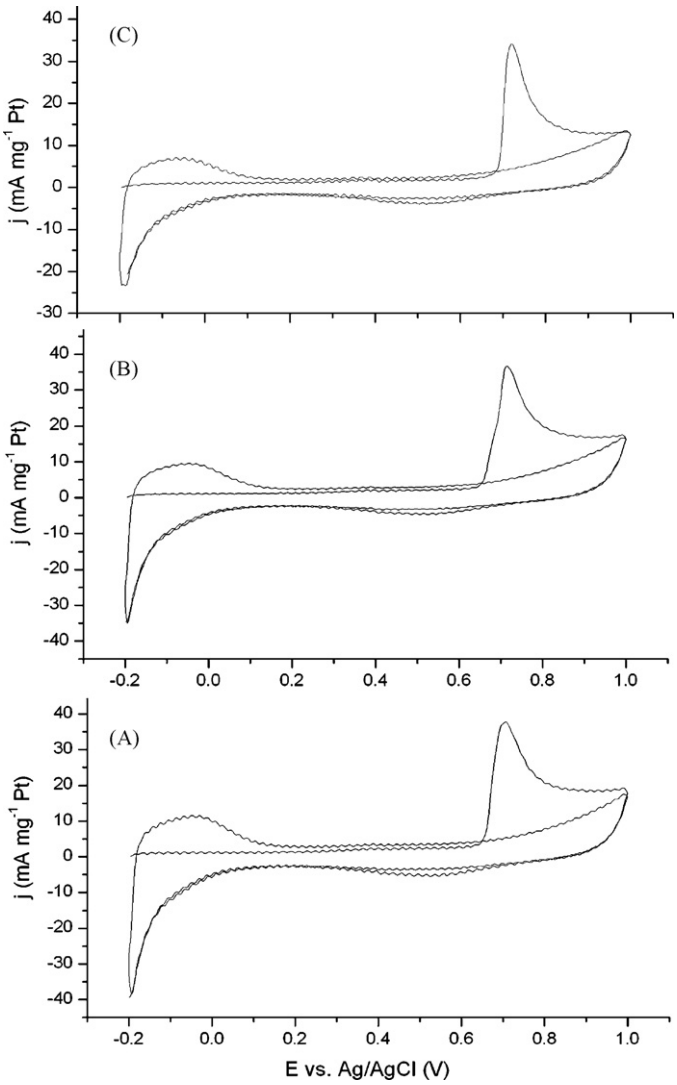

Fig. 6. CO_{ad} stripping voltammograms for the (A) Pt–WO_3/C-1, (B) Pt–WO_3/C-2, and (C) Pt/C catalysts at room temperature.

3.2. Electrochemical analysis

The electrochemically active specific surface area of catalysts can reflect the intrinsic catalytic activity of the catalysts. Typically, this can be measured with the H_{ad} stripping or the CO_{ad} stripping method. In this study, the CO_{ad} stripping method was used. Fig. 6 shows the CO_{ad} stripping voltammograms for the Pt–WO_3/C-1, Pt–WO_3/C-2 and Pt/C (C) catalysts. It can be seen from Fig. 6 that the peak potential for CO_{ad} oxidation at the Pt–WO_3/C-1, Pt–WO_3/C-2 and Pt/C (C) catalysts electrodes are 0.695, 0.712, and 0.723 V, respectively. The corresponding peak currents are 37.6, 35.8 and 34.1 mA mg^{-1} Pt. Furthermore, the electrochemically active specific surface area (ECSA) of Pt for all the catalysts can be calculated by using CO oxidation charge after subtracting the background current. It is 76.4, 69.3, and 58.1 $m^2\ g^{-1}$ for the Pt–WO_3/C-1, Pt–WO_3/C-2, and Pt/C (C) catalysts, respectively.

Fig. 7 depicts cyclic voltammograms (CV) of the catalyst samples performed in electrolytes of 0.5 M H_2SO_4 and 1 M CH_3OH at a scan rate of 20 mV s^{-1} with Pt loading of 0.14 mg cm^{-2}. It can be observed that the onsets of methanol oxidation all begin at about 0.3 V (vs. Ag/AgCl). The peak potentials for methanol oxidation are also similar, i.e., ~0.75 V (vs. Ag/AgCl). However, the oxidation peak for Pt–WO_3/C-1 is 254 mA mg^{-1} Pt, which is much higher than that

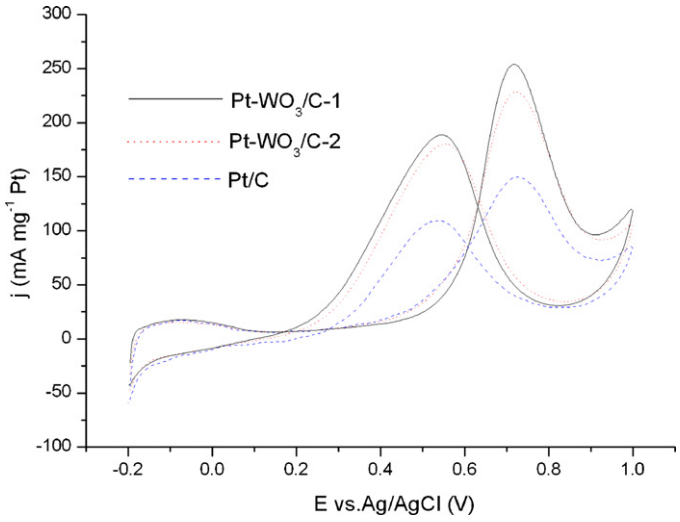

Fig. 7. Cyclic voltammograms recorded at 20 mV s^{-1} in 1 M CH_3OH + 0.5 M H_2SO_4 solution at room temperature.

of other sample (i.e., 224 mA mg^{-1} Pt for the Pt–WO_3/C-2 catalyst and 151 mA mg^{-1} Pt for the Pt/C catalyst). In other words, the Pt–WO_3/C-1 catalyst has a higher activity than the Pt–WO_3/C-2 and the Pt/C catalysts.

The chronoamperometry (CA) curves for the three catalysts are shown in Fig. 8. These curves reflect the activity and stability of the three catalysts to catalyze methanol oxidation. Obviously, the decay in the methanol oxidation current with time varies. The Pt–WO_3/C-1 catalyst has the highest initial current density and limiting current density, and therefore, has the best catalytic activity and stability.

This significant improvement in the catalytic performance of the Pt–WO_3/C catalysts may be attributed to two factors: first, the Pt and WO_3 particles supported on the carbon are smaller and more uniformly distributed; second, WO_3 is able to form a hydrogen tungsten bronze (H_xWO_3) compound in acid solution and this compound can facilitate dehydrogenation during methanol oxidation reaction. The methanol oxidation reaction is a six-electron-transfer reaction, with successive dehydrogenation steps followed by the removal of CO.

$$CH_3OH + H_2O \rightarrow CO_2 + 6H^+ + 6e^- \quad (2)$$

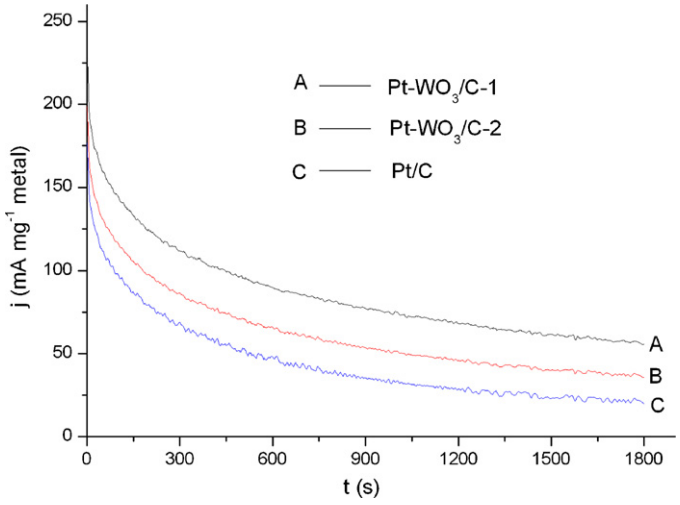

Fig. 8. Polarization current vs. time plots measured at room temperature in 1 M CH_3OH + 0.5 M H_2SO_4 solution at 0.6 V (vs. Ag/AgCl).

In the presence of WO_3, the hydrogen adsorbed on the Pt spills over onto the surface of the WO_3 and forms H_xWO_3, thus releasing these Pt active sites. Subsequently, H_xWO_3 can be readily oxidized to release hydrogen ions, electrons, and WO_3 [11,12,27–30]. This cyclic process will accelerate the dehydrogenation of methanol on Pt and lead to higher rate of methanol oxidation on the Pt–WO_3/C catalyst than on the Pt/C catalyst. The cyclic process on the Pt–WO_3/C catalyst is speculated to occur as follows [11,12]:

$$WO_3 + x\text{Pt–H} \rightarrow H_xWO_3 + x\text{Pt} \quad (3)$$

$$H_xWO_3 \rightarrow WO_3 + xH^+ + xe^- \quad (4)$$

Conclusion

A simple and novel method is proposed to prepare highly dispersed WO_3 by the adsorption and decomposition of PWA on carbon. The newly prepared WO_3/C is compared with the one prepared by conventional means with sodium tungstate as the precursor. TEM images show that the new method can produce a more uniform distribution and smaller average particle size of WO_3 particles on WO_3/C. Pt particles dispersed on the newly prepared WO_3/C samples are of average size (3.2 nm) and display the characteristic diffraction peaks of the Pt face-centered cubic structure. Electrochemical analysis shows that the Pt–WO_3/C catalysts prepared by this new method exhibit excellent catalytic activity and stability for methanol electro-oxidation. This significant improvement in the catalytic performance may be attributed to two causes: first, the Pt and WO_3 particles supported on carbon are uniformly distributed and have a smaller average size; second, the WO_3 is able to form the hydrogen tungsten bronze (H_xWO_3) compound in acid solution, which facilitates dehydrogenation during methanol oxidation reaction.

Acknowledgements

This work was supported by the High Technology Research Program (863 program 2007AA05Z159, 2007AA05Z143) of the Science and Technology Ministry of China and the National Natural Science Foundation of China (20933004, 21011130027 and 21073180). The authors are grateful for the help of Dr. Datong Song.

References

[1] X. Ren, T.E. Springer, T.A. Zawodzinski, S. Gottesfeld, J. Electrochem. Soc. 147 (2000) 466.
[2] C.H. Rhee, H.K. Kim, H. Chang, J.S. Lee, Chem. Mater. 17 (2005) 1691.
[3] H. Yang, T.S. Zhao, Q. Ye, Electrochem. Commun. 6 (2004) 1908.
[4] M. Watanabe, S. Motoo, J. Electroanal. Chem. 60 (1975) 267.
[5] M. Watanabe, S. Motoo, J. Electroanal. Chem. 60 (1975) 275.
[6] J.B. Goodenough, R. Manoharan, A.K. Shukla, K.V. Ramesh, Chem. Mater. 1 (1989) 391.
[7] T. Toda, H. Igarashi, H. Uchida, M. Watanabe, J. Electrochem. Soc. 146 (1999) 3750.
[8] K.-W. Park, J.-H. Choi, B.-K. Kwon, S.-A. Lee, Y.-E. Sung, J. Phys. Chem. B 106 (2002) 1869.
[9] K.-W. Park, J.-H. Choi, Y.-E. Sung, J. Phys. Chem. B 107 (2003) 5851.
[10] B.S. Hobbs, A.C.C. Tseung, Nature 222 (1969) 556.
[11] P.J. Kulesza, L.R. Faulkner, J. Electroanal. Chem. 259 (1989) 81.
[12] A.C.C. Tseung, K.Y. Chen, Catal. Today 38 (1997) 439.
[13] P.K. Shen, K.Y. Chen, A.C.C. Tseung, J. Electrochem. Soc. 142 (1995) L85.
[14] P.K. Shen, A.C.C. Tseung, J. Electrochem. Soc. 141 (1994) 3082.
[15] P.K. Shen, K.Y. Chen, A.C.C. Tseung, J. Chem. Soc. Faraday Trans. 90 (1994) 3089.
[16] X. Cui, J. Shi, H. Chen, L. Zhang, L. Guo, J. Gao, J. Li, J. Phys. Chem. B 112 (2008) 12024.
[17] S. Jayaraman, T.F. Jaramillo, S. Baeck, E.W. McFarland, J. Phys. Chem. B 109 (2005) 22958.
[18] D.Y. Zhang, Z.F. Ma, G.X. Wang, K. Konstantinov, X.X. Yuan, H.K. Liu, Electrochem. Solid State Lett. 9 (2006) A423.
[19] K.Y. Chen, P.K. Shen, A.C.C. Tseung, J. Electrochem. Soc. 142 (1995) L54.
[20] P.K. Shen, K.Y. Chen, A.C.C. Tseung, J. Electroanal. Chem. 389 (1995) 223.
[21] U.L. Štangar, N. Grošelj, B. Orel, P. Colomban, Chem. Mater. 12 (2000) 3745.
[22] Y. Takasu, T. Fujiwara, Y. Murakami, K. Sasaki, M. Oguri, T. Asaki, W. Suginoto, J. Electrochem. Soc. 147 (2000) 4421.

[23] T. Kawaguchi, W. Sugimoto, Y. Murakami, Y. Takasu, Electrochem. Commun. 6 (2004) 480.
[24] Y. Wu, X. Ye, X. Yang, X. Wang, W. Chu, Y. Hu, Ind. Eng. Chem. Res. 35 (1996) 2546.
[25] J.F. Moulder, W.F. Stickle, P.E. Sobol, K.D. Bomben, in: J. Chastain (Ed.), Handbook of X-ray Photoelectron Spectroscopy, Perkin–Elmer Corp., Eden Praire, MN, 1992.
[26] J. Rajeswari, B. Viswanathan, T.K. Varadarajan, Mater. Chem. Phys. 106 (2007) 168.
[27] B. Reichman, A.J. Bard, J. Electrochem. Soc. 126 (1979) 583.
[28] A. DiPaola, F. DiQuarto, C. Sunseri, Corros. Sci. 20 (1980) 1067.
[29] J.P. Randin, R. Viennet, J. Electrochem. Soc. 129 (1982) 2349.
[30] J. Ye, J. Liu, Z. Zou, J. Gu, T. Yu, J. Power Sources 195 (2010) 2633.